Aerosol Characteristics and Radiative Impacts over the Arabian Sea during the Intermonsoon Season: Results from ARMEX Field Campaign

K. KRISHNA MOORTHY AND S. SURESH BABU

Space Physics Laboratory, Vikram Sarabhai Space Centre, Trivandrum, India

S. K. SATHEESH

Centre for Atmospheric and Oceanic Sciences, Indian Institute of Science, Bangalore, India

(Manuscript received 8 May 2004, in final form 23 July 2004)

ABSTRACT

During the second phase of the Arabian Sea Monsoon Experiment (ARMEX-II), extensive measurements of spectral aerosol optical depth, mass concentration, and mass size distribution of ambient aerosols as well as mass concentration of aerosol black carbon (BC) were made onboard a research vessel during the intermonsoon period (i.e., when the monsoon winds are in transition from northeasterlies to westerlies/southwesterlies) over the Arabian Sea (AS) adjoining the Indian Peninsula. Simultaneous measurements of spectral aerosol optical depths (AODs) were made at different regions over the adjoining Indian landmass. Mean AODs (at 500-nm wavelength) over the ocean (~0.44) were comparable to those over the coastal land (~0.47), but were lower than the values observed over the plateau regions of central Indian Peninsula (~0.61). The aerosol properties were found to respond distinctly with respect to change in the trajectories, with higher optical depths and flatter AOD spectra associated with trajectories indicating advection from west Asia, and northwest and west-coastal India. On average, BC constituted only ~2.2% to total aerosol mass compared to the climatological values of ~6% over the coastal land during the same season.

These data are used to characterize the physical properties of aerosols and to assess the resulting short-wave direct aerosol forcing. The mean values were –27 W m^{-2} at the surface and −12 W m^{-2} at the top of the atmosphere (TOA), resulting in a net atmospheric forcing of +15 W m^{-2}. The forcing also depended on the region from where the advection predominates. The surface and atmospheric forcing were in the range −40 to −57 W m^{-2} and +27 to +39 W m^{-2}, respectively, corresponding to advection from the west Asian and western coastal India where they were as low as −19 and +10 W m^{-2}, respectively, when the advection was mainly from the Bay of Bengal and from central/peninsular India. In all these cases, the net atmospheric forcing (heating) efficiency was lower than the values reported for northern Indian Ocean during northern winter, which is attributed to the reduced BC mass fraction.

1. Introduction

The role of atmospheric aerosols in modifying the radiation budget of the earth–atmosphere system with implications to regional and global climate is being increasingly understood and recognized (Charlson et al. 1992; Hansen et al. 1997; Boucher et al. 1998; Haywood et al. 1999; Ramanathan et al. 2001). Nevertheless, there still persist large uncertainties in the regional radiative forcing caused by aerosols (Houghton et al. 2001). This arises mainly because of the lack of adequate knowledge of aerosol properties, and the large variations in these properties over rather short scales, both spatially and temporally. Over the land, this arises primarily from the wide variety of source processes, while over the ocean, transport from the continents contribute a major share (Prospero et al. 1983; Andreae 1995; Moorthy et al. 2003). Aerosols influence the radiation budget of the earth–atmosphere system broadly in two different ways. The first is the direct effect in which aerosols scatter and absorb the incoming solar and outgoing terrestrial radiations, thereby altering the radiative balance of the earth–atmosphere system (e.g., Haywood et al. 1999). While scattering (e.g., by sulfate aerosols) results in an increase in atmospheric albedo and a consequent decrease in the amount of radiation reaching the Earth's surface thereby causing a cooling effect (e.g., Charlson et al. 1992), aerosols such as black carbon (BC) and dust significantly absorb in the visible and IR spectrum leading to atmospheric warming and a surface cooling (e.g., Ramanathan et al. 2001). In the second, the indi-

Corresponding author address: K. Krishna Moorthy, Space Physics Laboratory, Vikram Sarabhai Space Centre, Trivandrum 695 022, India.
E-mail: k-k-moorthy@eth.net

rect effect, aerosols modify the microphysics and thereby the radiative properties and lifetime of clouds (Twomey 1977; Boucher et al. 1998; Heymsfield and McFarquhar 2001). Thus the radiative impacts of aerosols depend to a great degree on the relative abundance of these scattering and absorbing species. Significant variations in their abundance can occur regionally and seasonally at locations far away from potential sources as a result of changes in airmass types and prevailing meteorological conditions (Babu and Moorthy 2002). Observational studies have documented the importance of absorbing aerosols even in remote oceanic regions (Posfai et al. 1999). Even though numerous studies on the radiative effect of aerosols have focused on the role of anthropogenic sulphate (Charlson et al. 1992; Kiehl and Briegleb 1993; Tayler and Penner 1994; Chuang et al. 1997; Boucher et al. 1998; Capaldo et al. 1999), quantitative estimates of radiative forcing by BC is far less numerous (Haywood and Shine 1995; Haywood and Ramaswamy 1998; Babu et al. 2002). Scarcity of field measurements of BC, particularly over oceanic regions, makes it difficult to estimate their role in perturbing the aerosol radiative forcing over oceans. Comprehensive and multi-instrumental field experiments provide the answer to the above over a regional scale, even though they are limited in temporal and geographical extent.

In this context, the Arabian Sea (AS) assumes significance. This region is characterized by a distinct weather pattern associated with Indian monsoon; the winds associated with which reverse direction seasonally, followed by highly contrasting precipitation. It is also influenced by the anthropogenic activities along the densely populated west coast of India because of the close proximity and the seasonally changing synoptic air mass associated with the monsoons (Asnani 1993). Besides, long-range transport of aerosols from west Asia and southeast Asia is also known to modify the aerosol properties over the AS (Jha and Krishnamurti 1999; Moorthy and Saha 2000; Li and Ramanathan 2002; Satheesh and Srinivasan 2002). Prior to 1995, measurements of aerosols over AS were limited. Systematic, long-term, and all-season observations over this region made from the island station Minicoy (MCY; Moorthy and Satheesh 2000) during 1995–98, were, however, limited to spectral aerosol optical depths (AODs). Even though the recent international field campaigns under the INDOEX (Indian Ocean Experiment) have provided a considerable insight into the aerosol properties and their radiative impacts (Ramanathan et al. 2001; Moorthy et al. 2001), these studies were primarily conducted during the dry, Indian (northern) winter season, when the synoptic airmass was steady and continental in nature. Observations are sparse during other seasons (Vinoj and Satheesh 2003). Notwithstanding the absence of a variety of sources of aerosols over the oceans and the consequent homogeneity in their properties to a certain extent, unlike the case over the continents, significant spatial and temporal heterogeneity have been observed even on a comparatively short scale because of the impact of the adjoining continents, the changing airmass types, and long-range transport (Smirnov et al. 2002a; Sakerin and Kabanov 2002). This makes the need for spatially and temporally well-resolved measurements of various aerosol properties, simultaneously using multiple instruments, all the more important for more accurate characterization of aerosol radiative forcing. Such observational field data are scanty over the AS and Bay of Bengal (BoB) regions, particularly during the intermonsoon season (March–April) when the prevailing low-level circulations show a transition from the easterly/northeasterly winter circulations to the westerly/southwesterly summer circulations, associated with the northward migration of the intertropical convergence zone (ITCZ) and the southwest (or the summer) monsoon season (May–September).

In this paper, we report the results of simultaneous and collocated measurements of several aerosol parameters (spectral AOD, size distribution, BC mass concentration, and total aerosol mass concentration) over the AS (8°–12°N, 72°–77°E) and the adjoining Indian peninsula during the intermonsoon period of 2003. The data are used to characterize the physical properties of aerosols and to assess their impact on the short wave direct radiative forcing over the oceanic region. The role of long-range transport in modifying the aerosol properties and their consequence on the radiative impacts are explored and the results are discussed.

2. Experimental details and data

The investigations were carried out onboard oceanographic research vessel (ORV) *Sagar Kanya* during its cruise SK190, devoted to atmospheric and oceanographic studies of the AS as a part of Arabian Sea Monsoon Experiment (ARMEX) under the Indian Climate Research Program (ICRP). Even though the cruise was designed primarily for meteorological and oceanographic measurements, simultaneous and collocated measurements of columnar aerosol spectral optical depth (AOD), total (M_t), as well as size-segregated (m_c) aerosol mass concentrations and mass concentration (M_b) of aerosol BC, were carried out onboard to characterize aerosols.

Onboard spectral AOD measurements were made using a hand-held Microtops sunphotometer (Solar Light Co.) at wavelengths of 380, 500, 675, and 870 nm. The instrument, when manually aimed at the Sun, makes measurements of the direct solar irradiance and derive the AODs based on its internal calibration, and the observation coordinates and time as recorded using a global positioning system (GPS) receiver attached to it. More details of this instrument are available elsewhere (Morys et al. 2001). Adequate care was taken in

collecting these data onboard the ship following the necessary precautions and considerations (Ichoku et al. 2002). Since the instrument was manually operated, it was possible to select periods free from visible clouds to perform the measurements. As the sky was predominantly cloud-free over the AS during the cruise period, AOD data could be obtained on 24 days out of the 27 cruise days.

A 10-channel Quartz Crystal Microbalance (QCM) cascade impactor (model PC-2, California Measurements Inc.) was used for near–real-time measurements of the total mass concentration (M_t) as well as the mass-size distribution (m_{ci}) of ambient aerosols in the marine atmospheric boundary layer. The QCM makes size resolved measurements of aerosol mass concentration (m_{ci}) in its 10 size bins, having 50% cut off diameters at 25, 12.5, 6.4, 3.2, 1.6, 0.8, 0.4, 0.2, 0.1, and 0.05 μm for the stages i = 1–10, respectively. More details of the instrument, the data collection procedures, precautions taken, and error budget are given in an earlier paper (Pillai and Moorthy 2001). The sampling duration varied from 5 to 8 min depending on the aerosol loading. The instrument was kept at the bow side ship deck, just below the bridge, at ~10 m above the water level, and operated only when the ship was in motion at the normal cruising speed so that the instrument aspirates the clean oceanic air coming on to the ship, uncontaminated by the ship's exhaust or any possible ship-based emissions and only when the ambient RH<75%. A total of 143 measurements were made during the entire cruise period.

Continuous and near–real-time measurements of BC mass concentration (M_b) were made using an Aethalometer; model AE-21 of Maggie Scientific (Hansen et al. 1984). It converts the measured optical attenuation to M_b using an absorption efficiency of ~16 $m^2\ g^{-1}$, which is very close to the mean value (15 $m^2\ g^{-1}$) reported by Neusüß et al. (2002) during INDOEX. Field experiments have also shown excellent agreement of the Aethalometer measured M_b with those from other analytical techniques, such as the TOR (Im et al. 2001). The instrument was kept inside the ship's cabin and ambient air (from ~12 m above sea level) was taken through an inlet pipe from the front-end region (sampling into the wind) of the ship. The flow rate was 4 λ min^{-1} and time base 5 min, so that BC estimates were available at 5-min intervals, 24 h a day. Following the details on aethalometer error budget (Babu et al. 2004), for the configuration used in this study, the uncertainty in M_b was in the range 40–60 ng m^{-3} for each measurement at a 5-min interval.

The ORV sailed off from Mangalore (MNG; Fig. 1) on 14 March 2003 and after the campaign returned to Cochin (CHN) on 10 April 2003, following the track shown by the dotted line in Fig. 1. The filled circles denote the daily position of the ship at 0630 UTC on the date shown beside. At the position shown as TSL in the figure, the ship had time series observations of meteorological and oceanographic parameters from 23 March to 7 April (main objective of ARMEX). During this period the aerosol measurements were mostly restricted to columnar AOD.

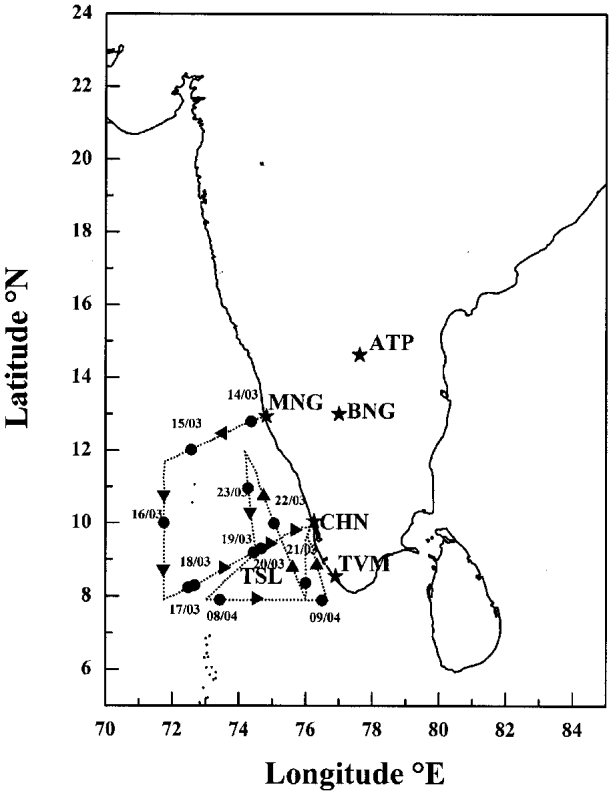

FIG. 1. Cruise track for SK190. The solid circles on the lines show the position of the ship at 0630 UTC on the dates shown. The point TSL is the time series location. The locations CHN and MNG represent Cochin and Mangalore where the cruise terminated and originated, respectively. At the locations TVM, BNG, and ATP (Trivandrum, Bangalore, and Anantapur, respectively) simultaneous AOD measurements were made using an MWR (details are given in the text).

3. Continental measurements

Besides the measurements made onboard the ship, simultaneous observations of spectral AOD were made over peninsular India from three stations, Trivandrum (TVM; 8.5°N, 77°E, 3 m MSL), Bangalore (BNG; 13°N, 77°E, 960 m MSL), and Anantapur (ATP; 14.62°N, 77.65°E, 331 m MSL) (all shown in Fig. 1) using a 10-channel multiwavelength solar radiometer (MWR) operating at 380, 400, 450, 500, 600, 650, 750, 850, 935, and 1025 nm. The instrument details, analysis procedure, and error budget are described in several earlier papers (Moorthy et al. 1997 2003). Estimates of AOD are all made on apparently clear days, and these data during the cruise period are used in this study.

4. General meteorology

a. Synoptic winds

The mean synoptic winds (at 850 hPa) over the region are shown in Fig. 2 for the months of March and April 2003. While to the north of ~20°N, weak westerlies prevail, weak easterlies are seen to the south, over the BoB, the peninsula, and the study region over the AS. A weak anticyclone over the north AS and the associated flows are conducive for advection from West Asia across the north AS and from central India over to central AS. Down south, the flow pattern also shows winds from the BoB to the south AS across the peninsula. Thus the synoptic winds show a transition (typical to the intermonsoon season) from the predominantly northeasterly winter circulation before changing over to strong southwesterlies associated with the Indian summer monsoon.

b. Meteorological parameters over the ocean

Information on the surface meteorological parameters was obtained from the shipboard measurements at every minute. These included wind speed and direction (corrected for ship's motion), relative humidity (RH), and temperature. These data are averaged at 6-h intervals and then smoothed using a 4-point running mean to get the average characteristics as shown in Fig. 3. It can be seen that the surface winds during the entire cruise period were generally weak (speed <5 m s^{-1}). During the initial part of the campaign, the winds were variable between land and sea (until 22 March) and there after it was mostly from the seaward side of the observation locations. Except for weak drizzles (on 19 and 20 March) there was no rainfall during the entire cruise period. The RH was in the range 62–80 with a mean value of ~70%.

5. Results and discussions

a. Spectral aerosol optical depths

AODs, measured onboard using the Microtops on each day, were averaged to get the daily mean AOD (a day typically had 20 measurements of AOD). The temporal variations of AODs, thus obtained and shown in Fig. 4 at the four wavelengths, reveal a gradual decrease from the moderately high initial values, to reach the lowest values during the cruise on 19 March 2003. This was not because the measurements being made farther away from the mainland as the ship was farthest from the mainland on 15 and 16 March, as can be seen from Fig. 1. There after, the AODs increased steadily and a rather broad peak was attained during 31 March–2 April 2003, when the mean AODs were as high as ~0.84 at 500 nm. During this period, the ship was mostly around the TSL location (Fig. 1) for the time series observations. Subsequently, the AODs decreased till the end of the cruise. No AODs were obtained on 3 and 4 April because of cloudy and highly hazy skies. Spectrally, AODs were highest at the shortest wavelength and decreased rapidly toward the longer wavelengths. The mean (± standard deviation) AODs during the cruise period are given in Table 1, which indicates that the spectral shape resembles more to those observed over continental environments, rather

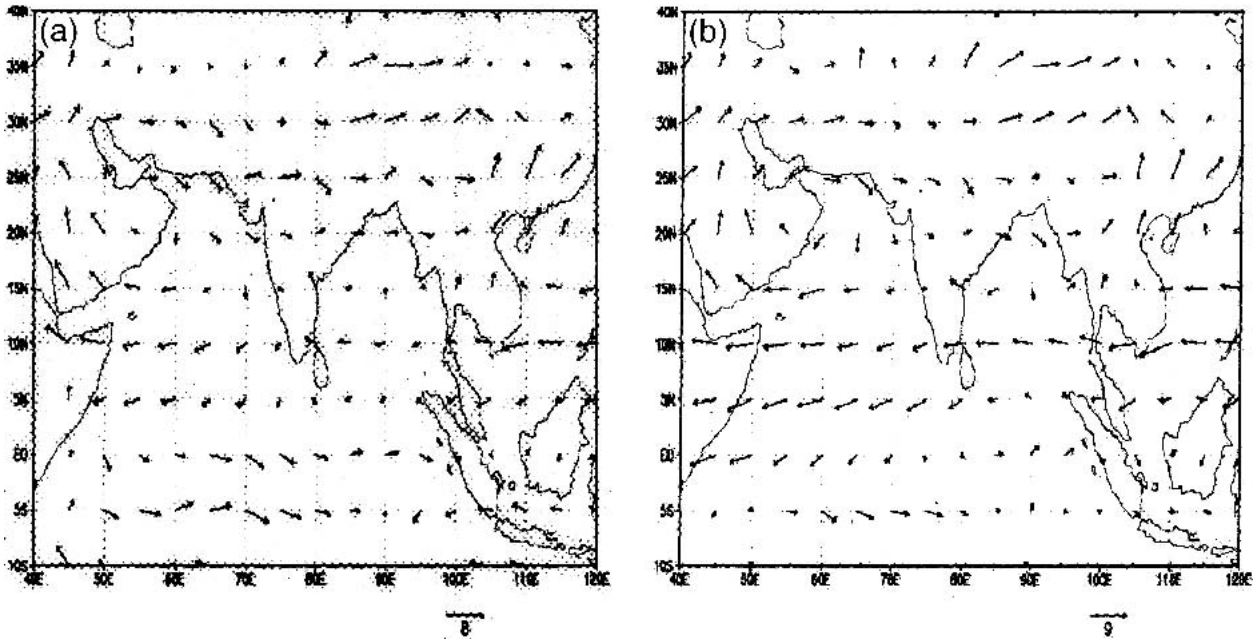

FIG. 2. Synoptic wind pattern over the Arabian Sea during (left) Mar 2003 and (right) Apr 2003.

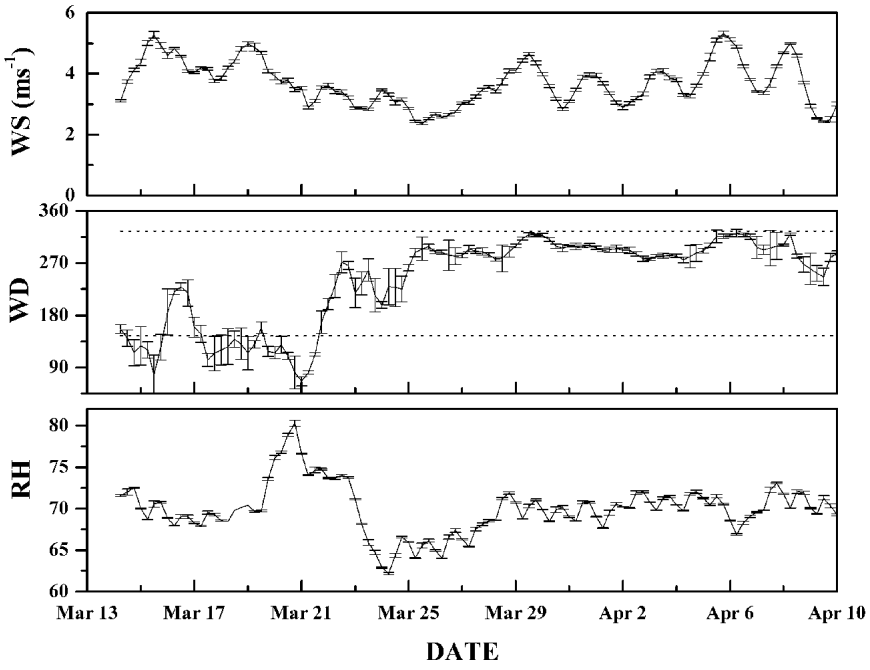

FIG. 3. Six-hourly (top) mean wind speed, (middle) wind direction, and (bottom) relative humidity onboard the cruise.

than the flat spectra generally expected within the marine environment. This indicates significant abundance of continental aerosols over the oceanic area under investigation. Since the ARMEX concentrated more on temporal features of atmospheric parameters associated with monsoon onset over the eastern AS, measurements were confined to a very small spatial extent and hence the spatial variations can be considered rather insignificant in comparison with the temporal changes.

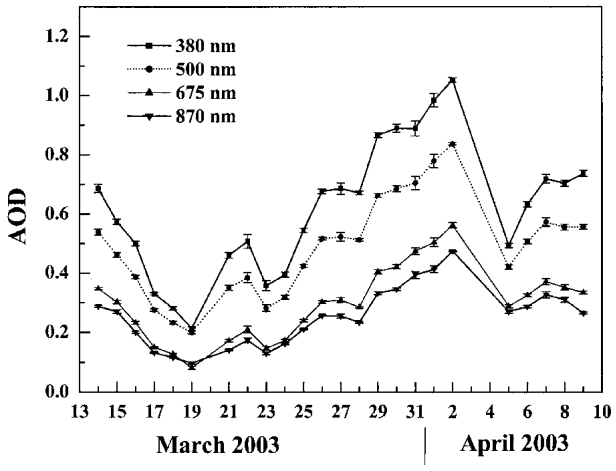

FIG. 4. Temporal variation of daily mean aerosol optical depth over the Arabian Sea at the four wavelengths

b. *Ångström parameters*

The spectral variation of AOD has within it the signature of the columnar size distribution of the aerosols. The steep increase in the AOD toward the shorter wavelengths is indicative of increased abundance of fine (submicron) aerosols. Inferences on the size spectra of the aerosols can be obtained readily from the corresponding AOD spectra [$\tau_p(\lambda)$] by estimating the Ångström parameters in the expression (Ångström 1964)

$$\tau_p(\lambda) = \beta\lambda^{-\alpha}, \quad (1)$$

where α is the wavelength exponent, which depends on the ratio of the concentration of large (coarse mode) to small (accumulation mode) aerosols; β is the turbidity coefficient, which depends on the total aerosol loading in the atmosphere and hence is dependent on the abundance of coarse aerosols (for the same or lower values of α); and λ is the wavelength in microns. Estimates of α and β were made by least squares fitting Eq. (1) to the measured AOD spectra on a log–log scale. Temporal variation of daily mean α for the cruise period is shown by the points in Fig. 5, with the vertical bars through them representing the error (standard deviation of the slope of the regression line) in α. In general, the values of α were in the range ~0.8–1.5 with a mean value of 1.17 ± 0.03. The solid line parallel to the abscissa in Fig. 5 represents this mean value, with the two dashed lines parallel to it showing the standard deviation from the mean. This value of α is generally comparable to the

TABLE 1. Mean AOD spectra during the campaign.

Wavelength (nm)	Mean AOD (± std dev)
380	0.565 ± 0.17
500	0.444 ± 0.13
675	0.267 ± 0.09
870	0.230 ± 0.09

values reported for coastal AS region in several earlier investigations (e.g., Satheesh and Moorthy 1997) but is higher than the value (~0.6) reported for far oceanic regions, implying increased relative dominance of accumulation mode aerosols.

However, the more interesting and important point is that the temporal variations of α were almost opposite in nature to those of the AODs, as can be seen from Fig. 6. Low values of AODs were associated with high values of α and vice versa, indicating that the increase in AOD is mainly because of the presence of coarse mode aerosols. This is further corroborated by the variation of β shown by the points joined by dashed line in the same figure, the variations of which are quite similar to that of the AOD. The coarse aerosols observed commonly over oceanic regions are either sea salt produced in situ by the winds or the transported mineral dust (Prospero 1979). Since the wind speeds during the entire cruise period were generally low (<5 m s^{-1}) and did not show any large increase around the periods of higher AOD (Fig. 3), it is unlikely that the sea-spray production mechanisms would have been responsible for the increase in AOD or β seen in Fig. 6. This suggests that long-range transport would be playing a significant role in producing the observed increases in AOD and decrease in α. This aspect will be examined in the subsequent section.

c. AODs over peninsular India

Aerosol properties over coastal oceanic regions would be significantly modified by the advection of aerosols from the adjoining landmass under favorable wind conditions. The continental nature of the prevailing air mass during the cruise period was conducive for such advection from the central and peninsular regions of India. With this in mind, we have examined the spectral AODs at TVM, BNG, and ATP (see Fig. 1 for the locations) during the campaign period. In Fig. 7 the mean AOD spectra for these stations are shown, along with that over the AS (dashed line). The vertical bars are the standard errors. A comparison of the AOD at 500 nm, α, and β for these stations with those from the cruise is given in Table 2. In the same table we have also given the mean values (for the same season) reported earlier for the neighboring locations such as the Kaashidhoo Climate Observatory (KCO; 4.965°N, 73.466°E) (Satheesh et al. 2002) and MCY (Moorthy and Satheesh 2000). The AOD at 500 nm observed over the cruise locations and over TVM are quite comparable,

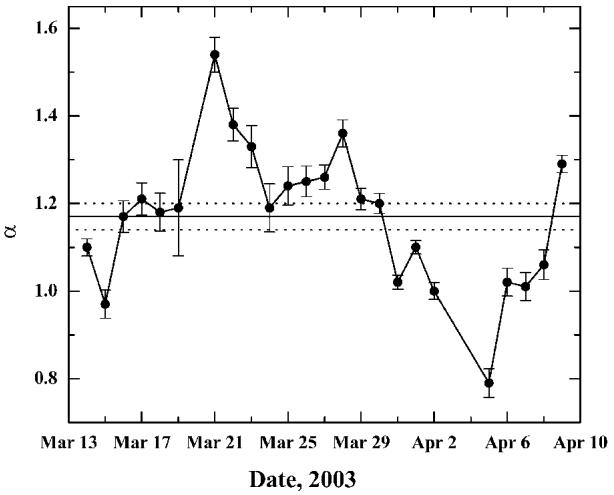

FIG. 5. Temporal variation of daily mean Ångström wavelength exponent estimated from the AOD spectra in Fig. 4. The solid line parallel to the abscissa represents the mean value of α and the dotted lines on either side of it represent the standard deviation of the mean.

but α value over AS is higher than that obtained for TVM. At BNG, an urban station at ~960 m MSL, the AODs are comparatively lower, but the spectrum yielded a value of α, which is higher than that seen at

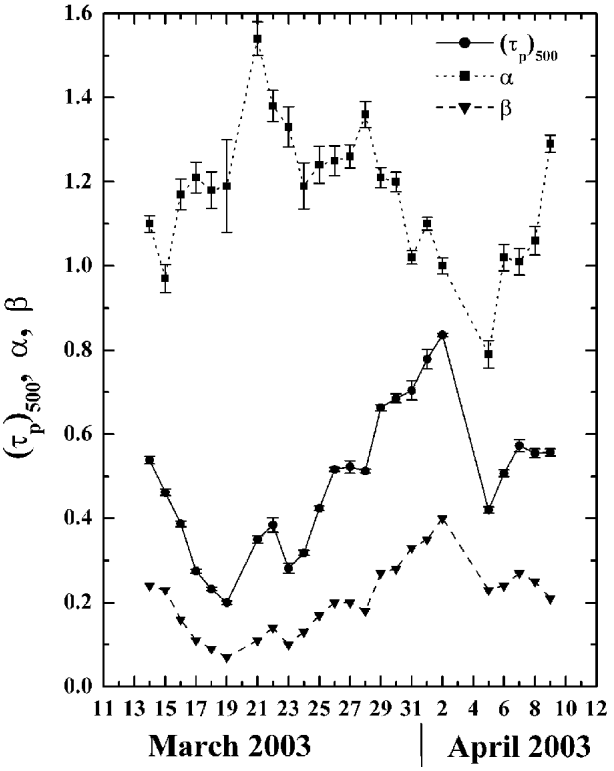

FIG. 6. Temporal variation of α and β along with τ_p at 500 nm, over the Arabian Sea.

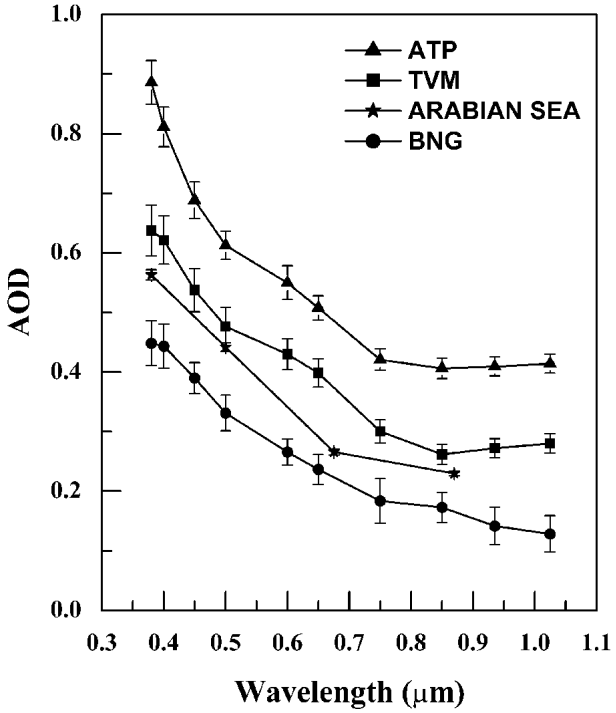

FIG. 7. Spectral variation of aerosol optical depth at different locations over peninsular India along with that observed over Arabian Sea during the study period.

TVM or the AS, thereby indicating enhanced submicron aerosol abundance, probably because of the large scale anthropogenic activities at this urban location. In contrast, the spectral AODs at ATP, which is a semiarid region, were higher than those at the other two stations, but the spectrum was more flat with a lower value for α and higher value for β (Table 2). Being a semiarid region, the high value of AOD associated with low value of α at ATP is indicative of the increased dominance of mineral dust, compared to the other two locations. The AODs at KCO and MCY are comparable to that observed during the cruise, but α values are higher indicating higher dominance of small aerosol at these locations (which lie farther away from the landmass).

d. Role of transport

The role of long-range transport of aerosols over the AS and Indian Ocean (IO) in causing changes in the optical depths, composition, and physical characteristics of aerosols has been investigated in the recent years, particularly during the INDOEX (Krishnamurti et al. 1998) and later over the BoB (Moorthy et al. 2003). Observations during the INDOEX have shown that aerosol properties over the AS are strongly influenced by aerosols advected from west Asia, Africa, and east/southeast Asia, besides those from the Indian landmass (Jha and Krishnamurti 1999; Moorthy and Saha 2000; Kamra et al. 2001; Li and Ramanathan 2002). The temporal variations of AOD, α, and β seen in Figs. 4–7 suggested possible nonlocal source effects.

TABLE 2. Comparison of aerosol properties.

Station	τ_{500}	α	β
Arabian Sea	0.44 ± 0.007	1.17 ± 0.03	0.21 ± 0.02
TVM	0.47 ± 0.032	0.99 ± 0.03	0.26 ± 0.02
BNG	0.33 ± 0.030	1.30 ± 0.001	0.13 ± 0.019
ATP	0.61 ± 0.023	0.80 ± 0.044	0.37 ± 0.02
KCO*	0.45	1.30	0.19
MCY	0.42	1.40	0.15

* From Satheesh et al. (2002).

With a view to examining this aspect, we computed the 7-day back trajectories for all the days on which the AOD data were available during the cruise, using the Hybrid Single Particle Legrangian Integrated Trajectory (HYSPLIT) model of the National Oceanic and Atmospheric Administration (NOAA; Draxler and Rolph 2003). The 7-day period was considered in view of the typical residence time of $\geq$1 week for aerosols in the lower troposphere, reported for this region (Ramanathan et al. 2001) during the dry period. As the AOD values are caused by the columnar aerosols, we considered three height levels over the observation site based on the marine boundary layer (MBL) characteristics of INDOEX (Manghnani et al. 2000): 500 m (within the MBL), 1800 m (above the MBL but below the trade wind inversion level), and 3600 m (in the lower free troposphere; Moorthy et al. 2003).

The isentropic trajectories revealed significant variations, particularly at the lower levels, during the cruise period. The highest, free tropospheric (FT) trajectory was generally confined to the central and peninsular India for at least 3 days before arriving the observation site. Nevertheless, in some cases the FT trajectories originated from the west Asian countries and traveled across Pakistan and northwest India before arriving at the central and peninsular Indian regions, while on other occasions they originated from the BoB and traveled along the east coast of India and across the peninsula to reach the observation site. Yet, on several days the FT trajectories were mainly confined to the Indian landmass for all 7 days. At the lower levels, the trajectories showed three main routes: (i) predominantly from the west Asian regions, north and western India, the west coast India, and across the AS; (ii) from east coast of India, part of BoB, and the peninsular regions; and (iii) originating from the central or east BoB, reaching the Indian peninsula after a considerable oceanic travel, and then crossing the peninsula to the observation site. Thus, broadly the trajectories could be classified into six groups depending on their regional travel, as shown in Fig. 8. Groups 1–3 have the FT trajectory confined mainly to the Indian landmass, while the trajectories at the lower levels varied from

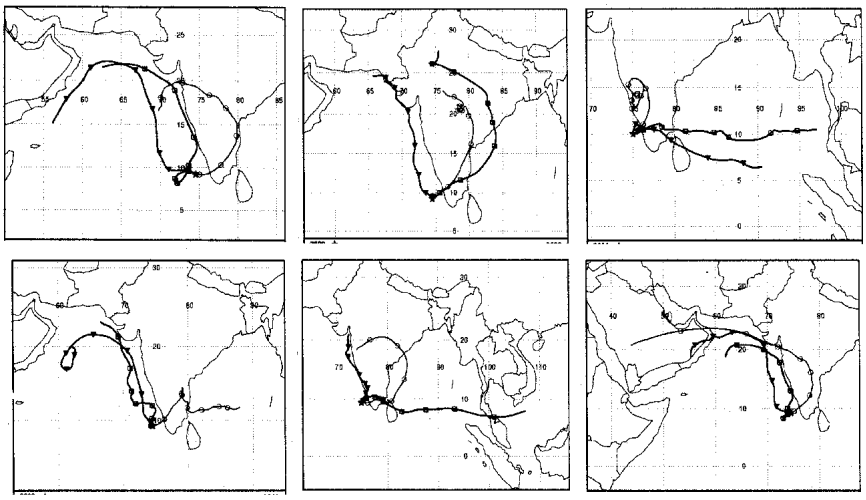

FIG. 8. Examples of back trajectories showing the different cases explained in Table 3. The frames from left to right correspond, respectively, to (top) groups 1, 2, and 3; (bottom) groups 4, 5, and 6.

west to east. In groups 4 and 5, the free tropospheric trajectory had a significant BoB history (for 2–4 days) before reaching India and then the observation point across India, while the lower trajectories, showed regional distinctiveness. In group 6, all the trajectories originated from the west Asian region and traveled across coastal AS or the western coastal landmass of India. The different groups considered above and their distinctiveness with respect to the regional coverage are given in Table 3.

Having classified all the trajectories into one of the above, the AOD spectra, α, and β for each observational day were put into the appropriate trajectory group and averaged. The results are given in Table 4. The most important finding is that when the trajectories (at least one of the high-level ones) have a significant history over the BoB region, the AODs tend to become lower, the spectra become steeper, and β becomes smaller, whereas when the trajectories cover more of west Asia and west and coastal India across the AS, the AODs become remarkably higher, with a much flatter spectrum and larger values of β. In fact the highest mean AODs (0.81 at 500 nm), highest β ($\sim$0.35) and flattest AOD spectra (mean $\alpha = 1.01$) were observed when all the three trajectories originated from the west Asian regions and traveled the western continental landmass, including western Indian coast or coastal AS (group 6), while the lowest AODs (mean 0.32 at 500 nm), lowest β ($\sim$0.11), and steepest spectra ($\alpha = 1.44$) occurred when both the lower trajectories had significant history over the BoB before traveling across the peninsula to the observation point (group 3). The other groups fell between these two extremes such that the more the trajectories are to the west, the AODs tend to become higher and α lower, as can be seen from Table 4. The trajectories with predominantly Indian influence (groups 2 and 5) come in between. This distinctiveness of α between the BoB and the AS regions was reported earlier by Satheesh et al. (2001), with the former indicating higher values of α. Based on observations from Port Blair in the BoB, Moorthy et al. (2003) observed that the AOD spectra become flatter when the air trajectories show significant advection from west Asia/Arabia and across India. The present findings, in addition to corroborating the above, very clearly suggest the following.

TABLE 3. Trajectory groups and their regional coverage.

Free tropospheric trajectory (3600 m)	Group	Middle-level trajectory (1800 m)	MABL trajectory (500 m)
Confined mainly to central and peninsular India	1	West Asia and west coastal India	West Asia and Arabian Sea
	2	BoB and peninsular India	West Asia and coastal India
	3	BoB and peninsular India	BoB and peninsular India
Has a strong BoB history prior to along with Indian component	4	West Asia and coastal or peninsular India	West Asia, Arabian Sea, or west coastal India
	5	BoB and peninsular India	West coastal India and Arabian Sea
Originating from west Asia, across western continents, and then across central India	6	Originating from west Asia and then across northwest India	Originating from west Asia and west coastal India and Arabian Sea

1) Aerosols, advected from the west Asian and (west and coastal) Indian landmass, across the AS, are distinctly different from those advected across the BoB.
2) The former contains a relatively higher abundance of coarse mode particles, while the latter is richer in accumulation mode particles, irrespective of the fact that they cross the Indian peninsula to reach the AS.
3) Higher AODs are associated with advection from the west rather than the east or central India. AODs tend to increase when at least one of the trajectories shows significant western continental influence.
4) The peak in the temporal variations (Fig. 4) occurred when all the trajectories came from west Asian region and traveled across Afghanistan/Pakistan and western India, while during periods when the AODs were low, the trajectories showed significant advection from the bay across Indian peninsula.

Examining the above observations from the geographical distinctiveness of these regions, it follows that significant amount of mineral dust transport from the western regions would be responsible for the high AODs and flatter AOD spectra seen over the AS. Potential west Asian impact over AS has also been reported by earlier studies (Husar et al. 1997; Moorthy and Saha 2000; Vinoj and Satheesh 2003). The significance of mineral dust transport over the AS has also been highlighted by Li and Ramanathan (2002) for the Indian summer season (June–August), but our studies show that these are significant even in the intermonsoon season. This change in the AOD and its spectral dependence related to advection has significant impact on the (regional) direct aerosol forcing as will be seen later.

e. Diurnal variations in AOD vis-à-vis advection

The air-back-trajectory analyses just described also revealed that the shift in the advection was gradual. Initially, when the AOD decreased toward the minimum, the advection revealed increasing influence from the east (BoB, across the peninsula) with the trajectory group changing from 4 to 5, until 20 March, when all the trajectories arrived from the east. After that the trajectories start shifting toward west, progressively becoming more westward, changing from group 5 to 4 to 3 to 2 by 25 March, and to group 1 by 28 March before all the trajectories becoming westerlies (group 6) by 1 April. This change in the advection region and the consequent change in the aerosol type could have short-term signatures on the AOD as well (e.g., Kaufman et al. 2000; Smirnov et al. 2002b). This aspect was examined by computing the diurnal variations in the AOD (using the individual AOD measurements made using the Microtops in each day) as the percentage deviation of the instantaneous AOD in a day from the mean AOD for that day. These have been done for all the days and the results have been examined for their distinctiveness (or otherwise) with respect to the trajectory groups.

TABLE 4. Trajectory mean AOD and Ångström parameters.

Trajectory group	Mean AOD at 500 nm	α	β
1	0.40 ± 0.05	1.05 ± 0.1	0.19 ± 0.06
2	0.49 ± 0.04	1.21 ± 0.04	0.21 ± 0.02
3	0.32 ± 0.05	1.44 ± 0.10	0.11 ± 0.01
4	0.57 ± 0.07	1.03 ± 0.07	0.27 ± 0.03
5	0.33 ± 0.1	1.22 ± 0.06	0.12 ± 0.08
6	0.81 ± 0.03	1.01 ± 0.01	0.38 ± 0.03

Results showed that when the trajectories showed significant advection from the east (from BoB, across Indian Peninsula; groups 3, 4, and 5) AODs show large diurnal variations as much as 30%–35%; decreasing from ~+15% (up the mean) in the forenoon period (FN) to ~−20% (down the mean) in the afternoon (AN), even though the mean AODs were only moderate (0.2–0.4 at 500 nm). However, as the trajectories shifted to more westerlies favoring advection of mineral dust, (groups 2 and 1) the diurnal variations perceptibly decreased to with in ±7% of the mean, the AODs became higher (~0.4–0.6); yet generally decreasing toward the AN. On days when the advection was entirely westerly (group 6), AOD were very high (>0.6 at 500 nm), the diurnal variations were within ±5%, and the AODs tend to increase in the AN.

Diurnal variations in AOD have been of recent scientific interest. Examining the diurnal variations in AOD from several AERONET sites, Smirnov et al. (2002b) have reported large diurnal variations (up to 40%) at locations influenced by urban and industrial activities, while at locations influenced by mineral dust outflow the diurnal variations are only within ±5%. From a similar study, more recently, from dust source regions of China, Wang et al. (2004) reported a season-independent diurnal variation exceeding ±10% of the mean, with larger AODs in the AN period. Our results during significant dust advection resembles the diurnal pattern reported by Wang et al. (2004) but is of much smaller amplitudes that are close to those reported by Smirnov et al. (2002b). This could be possibly because of the fact that our observations are made at locations quite far away form the potential dust sources. However, when advection was across Indian landmass (lying much closer), the diurnal variability was larger.

f. Near-surface aerosol characteristics

Characteristics of near surface aerosols were obtained from the QCM data. During each measurement, the QCM provided the total mass concentration (M_t) of ambient aerosols in the size range 0.05–25 μm and the mass concentration (m_{ci}) in each of its size bins ($i = 1, 10$). The QCM data can be effectively used to retrieve various physically meaningful parameters of aerosols such as accumulation (particles with

diameter $<\sim 1$ μm) and coarse (particles with diameter $>\sim 1$ μm) mode mass concentrations and effective radius (Pillai and Moorthy 2001; Ramachandran and Jayaraman 2002).

Aerosols in the coastal oceanic regions would be mixture of those of marine and continental origin; the former will have a strong coarse mode, while the latter would be richer in accumulation mode aerosols. In view of this, we have separated M_t into M_a and M_c, where M_a is the mass concentration in the accumulation size range and M_c that in the coarse size range, such that

$$M_t = M_a + M_c. \quad (2)$$

For the configuration of the QCM,

$$M_c = \sum_{i=2}^{6} m_{\mathrm{ci}} \text{ and } M_a = \sum_{i=7}^{10} m_{\mathrm{ci}}. \quad (3)$$

Using the mass size distribution, an estimate of the effective radius (R_{eff}), which is the area-weighted volume of aerosols, is also made. The mean values of M_t, M_c, M_a, and R_{eff} over AS during the cruise period are given in Table 5. The climatological values of these parameters at the coastal station TVM are also given in the same table for comparison. From Table 5, it can be seen that the mass concentration (M_t) of the composite aerosols over the AS is less than that observed at Trivandrum during either continental air mass period (November–February) or marine air mass period (June–September). Moreover, M_c is significantly higher than M_a, similar to what is seen at TVM during periods of marine air mass. This is synonymous with the high value of β seen in Table 1 and signifies abundance of coarse aerosols in the marine environment. This, along with the trajectories indicates that these should be partly caused by the sea spray and partly caused by transported mineral dust (particularly at higher levels). However, an examination in terms of the trajectories, did not reveal any distinct difference for the near surface aerosol concentration or size distribution.

g. Aerosol black carbon

Aerosol black carbon is by far the most important aerosol species contributing to aerosol absorption and has an important role on the global radiative forcing BC (e.g., Haywood and Shine 1995). The very small size range, coupled with its relative chemical inertness and hydrophobic nature, provides a longer residence time for this species in the atmosphere even in humid environments, making it amenable to long distance transport. Mass fraction of BC to the total aerosol mass concentration is very important in modeling aerosol radiative properties (Babu et al. 2002). However, there are no measurements of BC over the AS, closer to India. Thus the simultaneous measurements of M_t, and M_b in the cruise were used to characterize BC and to estimate its relative abundance. A mass plot of M_t versus M_b using simultaneous observations is shown in Fig. 9. The slope of the regression line through the origin yielded the mean mass fraction of BC as 2.2 ± 0.32%. (Following the error budgeting discussed in Babu and Moorthy 2002, the overall uncertainty in the mass fraction is ~14% of the mean value). This is significantly lower than the mean value (~7%–10%) reported at the adjacent coastal location, TVM, for the same season (Babu and Moorthy 2002), and also the mean value (6%) reported for KCO during 1998 (Satheesh et al. 1999), even though it is higher than that normally reported values for pristine oceanic regions (Hess et al. 1998). This low BC fraction would have a corresponding impact on the aerosol radiative forcing over the AS.

The mass concentrations of BC and composite aerosols, did not show any perceptible dependence on the region of advection. This might be probably cause by either the advection was dominating at higher levels or within the boundary layer the species are well mixed. This aspect can be resolved only by getting altitude profiles of aerosols (using aircrafts, for example) and such measurements are needed in future for improving the impact assessment.

h. Estimation of aerosol direct radiative forcing

The above characteristics of aerosols were used to estimate direct short wave radiative forcing over the AS

TABLE 5. Near-surface aerosol parameters observed and derived from QCM data.

No.	Parameter	Arabian Sea	Trivandrum (climatology)	
			Continental air mass	Marine air mass
1	M_t (μg m^{-3})	29.7 ± 1.13	51.48 ± 2.30	35.49 ± 1.35
2	M_c (μg m^{-3})	18.2 ± 0.86	15.55 ± 0.91	22.98 ± 1.12
3	M_a (μg m^{-3})	11.5 ± 0.47	35.93 ± 1.90	12.51 ± 0.59
4	R_{eff} (μm)	0.21 ± 0.01	0.22 ± 0.02	0.28 ± 0.01

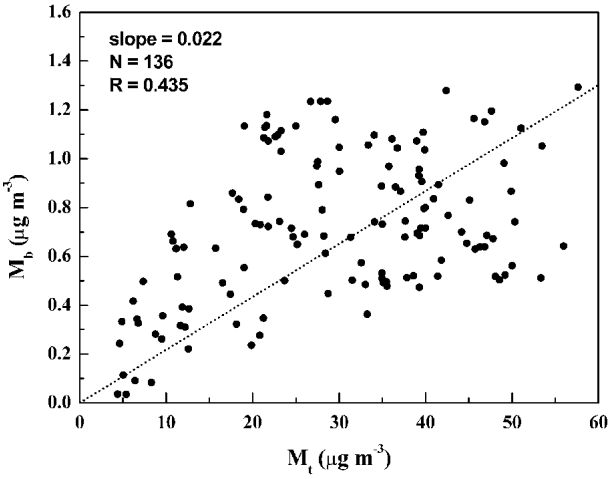

FIG. 9. Scatterplot showing the variation of total aerosol mass concentration (M_t) with that of BC mass concentration (M_b).

during the intermonsoon season, compare it with the earlier estimates elsewhere as well as those made over northern IO during winter season, and to examine the variability. For this we used the available observations as anchoring points in a marine aerosol model, which is fine-tuned to match the optical properties with the measurements. The optical and radiative properties, estimated from this model were then fed to a radiative transfer code.

Based on our observations of AOD, α, M_t, and M_b, we adopted the maritime polluted model of Hess et al. (1998) and used the BC mass fraction, spectral AODs, and α as the anchoring points in it. The Hess et al. model is based on a broad database obtained from different environment and describing the major aerosol composites as continental (clean and polluted), urban, desert, marine (clean and polluted), etc. The components of the selected model were sea salt (coarse and accumulation modes), water-soluble (nitrates, sulphates, etc.), and transported mineral dust, besides soot (BC). The concentrations of each of these species were adjusted, maintaining the BC mass fraction to the observed value of 2.2%, and following the considerations given in Satheesh et al. (1999), Lubin et al. (2002), Markowicz et al. (2003), and Vinoj et al. (2004), the optical properties of this modeled composite aerosol were estimated, assuming spherical aerosols, externally mixed. Pilnis et al. (1995) have shown that the nature of the state of mixing of aerosol is not very significant on SW radiative forcing. Moreover, for the INDOEX aerosol model, the global fluxes at the surface under clear skies, calculated for both externally and internally mixed aerosols were found to agree within 0.5% (Podgorny et al. 2000). The relative abundance of the nonmeasured species were varied such that the spectral AODs estimated for the composite aerosol model agreed well with the measured values in general and the value of α agreed with in 5% to the values obtained from measurements. The ambient RH was kept at 70% in the model, inline with the mean value observed during the cruise (Fig. 3). The resulting aerosol model had 57.4% water soluble components, 2.22% of soot (measurement), 19% of sea salt in accumulation size range, 19.2% of sea salt in coarse size range, and 2.3% of transported mineral dust by mass.

1) Estimated optical properties

Using the above aerosol model, the optical depths caused by the individual species and the cumulative AOD caused by the composite aerosols were estimated. The values of the AODs (total) thus estimated are compared with the measured values at the four wavelengths in Table 6, which shows a good agreement at all the wavelengths except at 675 nm. Nevertheless, the model-estimated value of α (1.19) agreed well (within 2%) with the mean value of 1.17 ± 0.03 obtained from the measurements (Fig. 5). The model estimated AODs for each of the aerosol species considered here showed that the water-soluble components contributed ~78% to the composite AOD, while soot contributed 8.8%, even though it is only 2.2% to the total aerosol mass. Yet, it is lower than the reported 11% share during INDOEX (Satheesh et al. 1999).

TABLE 6. Estimated and observed AODS.

Wavelength (nm)	Estimated AOD	Observed AOD
380	0.562	0.565 ± 0.17
500	0.441	0.444 ± 0.13
675	0.321	0.267 ± 0.09
870	0.212	0.230 ± 0.09

Using this composite aerosol model the single scattering albedo (ω) and phase function were estimated as a function of λ. The value of ω at 500 nm for the composite aerosol was ~0.92 ±0.01. This value is close to, but higher than the mean value of ~0.90 reported by Jayaraman et al. (2001) over the AS. Based on KCO observations, Satheesh et al. (1999) have reported a value of 0.9 during INDOEX 1998, whereas Ramanathan et al. (2001) reported a value of 0.86 ± 0.08 for the west coast of India and 0.89 ± 0.02 for AS. Our value of ω is higher than those reported for this region during INDOEX caused by the reduced BC mass fraction. Both, TARFOX and ACE-2 found a fairly wide range of values for ω at 550 nm, with $0.85 \leq \omega_{550} \geq 0.99$ for the marine aerosol impacted by continental pollution (Russell et al. 2002).

2) Radiative forcing

Radiative forcing is the change (ΔF) in the net flux (F), either at the top of the atmosphere or at the surface (S) as the case may be, because of a change in the environment. Such a change shall be produced by a change in atmospheric composition, nature of the constituent species, cloudiness, or surface properties. In the case of aerosol direct forcing,

$$(\Delta F)_{\mathrm{TOA,S}} = (F_{\mathrm{NA}})_{\mathrm{TOA,S}} - (F_{\mathrm{A}})_{\mathrm{TOA,S}}, \qquad (4)$$

where F_{A} and F_{NA} are respectively the net fluxes with and without aerosols. The net atmospheric forcing is defined as

$$(\Delta F)_{\mathrm{A}} = (\Delta F)_{\mathrm{TOA}} - (\Delta F)_{\mathrm{S}}. \qquad (5)$$

If the sign of ΔF_{TOA} is negative, the aerosol causes a net loss of radiative flux to the atmosphere leading to a cooling, while if it is positive, there will be a warming.

To compute (ΔF) we have used the discrete ordinate radiative transfer model, SBDART (Santa Barbara DISORT Atmospheric Radiative Transfer; Ricchiazzi et al. 1998). It is a detailed plane-parallel radiative transfer code based on the discrete-ordinate approach (Stamnes et al. 1988). The experimental values of spectral AOD and α, along with the estimated values of ω and phase function were incorporated into the SBDART to estimate the diurnally averaged, short-

wave, clear-sky, aerosol radiative forcing at the surface and TOA. The clear-sky assumption was well in line with the sky conditions generally prevailed during the cruise over the study region. Computations were performed for the wavelength range 0.25–4.0 μm as a function of solar zenith angles and the resulting fluxes were averaged over 24 h (Xu et al. 2003) and the forcing ΔF were estimated. A wavelength dependent ocean surface albedo was used, which was ~0.04 in the short wavelength end up to ~0.5 μm, increased a little to reach a peak value of ~0.061 at 0.58 μm, then gradually decreased to reach 0.0 at ~0.77 μm, and remained so for the entire longer wavelength region. The resulting diurnally averaged mean (range in brackets) aerosol forcing were 27 (−25.7 to −28.3) W m^{-2} at the surface $(\Delta F)_S$, and ~−12 (−11.6 to −12.3) W m^{-2} at the TOA $(\Delta F)_{TOA}$, is for the mean spectral AOD (0.44 at 500 nm) observed during the cruise. This amounts to an atmospheric forcing $(\Delta F)_A$ in the range 13.4–16.7 W m^{-2} with a mean value of +15 W m^{-2}. The surface forcing estimated over AS in the present study is quite comparable to the –26 W m^{-2} estimated by the TARFOX for the western North Atlantic Ocean. Translating our forcing estimates to forcing efficiencies (forcing for unit AOD) the mean values (range given in brackets beside) are –61 W m^{-2} for the surface, –27 W m^{-2} for TOA, and +34 (+30 to +38) W m^{-2} for the atmosphere. Using INDOEX-1998 campaign data, Podgorny et al. (2000) reported aerosol forcing efficiency values of −82 W m^{-2} for the surface, –20 W m^{-2} for the TOA, and 62 W m^{-2} for atmosphere over IO, while Satheesh and Ramanathan (2000) reported the forcing efficiency at the surface to be in the range –70 to –75 W m^{-2} and at the TOA to be –22 to –25 W m^{-2} over same region and season, but for 1999. The TOA forcing efficiency observed in our study is somewhat higher than the winter values, whereas the surface and net atmospheric forcing efficiencies are significantly lower even if we consider the upper bounds of our estimates. The ratio of surface to TOA forcing is only 2.25 in our study, compared to the value of ~3 reported by Satheesh and Ramanathan (2000). Absorbing aerosols result in an increase in the net atmospheric forcing (heating). Higher ratios (S/TOA) imply greater absorption. In the hypothetical cases of sea salt only or sulfate only aerosols, S/TOA is ~1.3 and ~1.6, respectively (Satheesh et al. 2002). Thus, the large reduction in the atmospheric forcing (and efficiency) over the AS seen in our study is attributed to the large decrease in the BC mass fraction during the intermonsoon season.

The net atmospheric forcing indicates the amount of radiative flux absorbed by the atmosphere caused by the presence of aerosols. This energy is converted into heat. The resulting atmospheric heating rate is (Liou 2002):

$$\frac{\partial T}{\partial t} = \frac{g}{c_p}\frac{\Delta F}{\Delta P}, \tag{6}$$

where $\partial T/\partial t$ is the heating rate (s^{-1}), g is the acceleration caused by gravity, C_p the specific heat capacity of air at constant pressure (~1006 J kg^{-1} K^{-1}), and P is the atmospheric pressure, respectively. The atmospheric absorption estimated in the present study thus translates into a heating rate in the range 0.38–0.47 K day^{-1} with a mean value of ~0.42 K day^{-1} (for ΔP = 300 hPa). Here it is to be emphasized that this heating rate is only a theoretical, static, 1D estimate, and is caused by absorption of short wave flux only. More realistic estimates should consider the long wave part as well as boundary layer processes.

Based on measurements over the AS, Vinoj and Satheesh (2003) reported shortwave aerosol direct forcing efficiencies of –37.5 W m^{-2} for the TOA, –43.75 W m^{-2} at the surface, and +6.25 W m^{-2} for the atmosphere, during summer monsoon season (July–August). It might be noticed that their values of atmospheric forcing are still lower than the values from the present investigation, and we attribute this to the change in the airmass type. Our observations fall during the intermonsoon season, when the winds are in a transition from the northeasterly winter circulation to the westerly/southwesterly. Thus, the aerosol forcing shows a significant change with season associated with the changes in the aerosol characteristics.

i. Impact of transport

The role of long-range transport of aerosols in modifying the aerosol properties over AS has been shown in the earlier section (5b). Significant enhancement in the AOD along with a flattening of the AOD spectra were noticed when the trajectories arrived from the western landmasses [including west Asia, western India, westcoastal India, and coastal (eastern) AS; group 6 in Table 3], while the AODs were very low and the spectra were steep when the trajectories were from the BoB across peninsular India (group 3 in Table 3) and the pattern was in between when they were mainly from the central/north Indian regions. Attributing these to a change in the aerosol composition and size distribution, we examined the impact of this on the mean radiative forcing estimates. Following the procedure just described the forcing components are estimated for each trajectory group detailed in Table 3. These are then normalized to the corresponding AODs to estimate the efficiencies. This is done because the absolute forcing depends on the value of the AOD and its spectral dependence as well as the composition of the aerosols, which determines ω. The changes in the direction of the advection (trajectory group) changes both and hence the actual impact on radiative forcing will be determined by the absolute magnitudes of ΔF; the efficiencies will give a measure of the sensitivity of the changes in the composition for the hypothetical case of the AODs remaining the same. The results are given in Table 7 for the different trajectory groups considered in this study. It is to be noted that the both, the forcing

TABLE 7. Change in aerosol forcing (W m^{-2}) and forcing efficiencies (normalized to the AOD) with respect to changes in trajectory.

Trajectory group	Mean AOD at 500 nm	α	Aerosol direct forcing (W m^{-2})			Corresponding forcing efficiencies		
			TOA	Surface	Atmosphere	TOA	Surface	Atmosphere
1	0.40 ± 0.05	1.05 ± 0.1	−10.61	−28.9	+18.29	−26.53	−72.25	+45.73
2	0.49 ± 0.04	1.21 ± 0.04	−13.39	−30.47	+17.08	−27.33	−62.18	+34.86
3	0.32 ± 0.05	1.44 ± 0.10	−9.15	−18.91	+9.76	−28.59	−59.09	+30.50
4	0.57 ± 0.07	1.03 ± 0.07	−14.03	−39.71	+25.68	−24.61	−69.67	+45.08
5	0.33 ± 0.1	1.22 ± 0.06	−9.52	−21.11	+11.58	−28.49	−63.57	+35.09
6	0.81 ± 0.03	1.01 ± 0.01	−18.03	−56.81	+38.78	−22.25	−69.71	+47.46

and forcing efficiency change significantly between the two extreme cases. The highest values for atmospheric forcing and efficiency are associated with trajectories bound from the western region (group 6) and the lowest values occur when they are from the east (group 3). It is interesting to note that the cases, when the advection is primarily from the Indian landmass, come in between these extremes, in spite of having a closer proximity to the observation site. In terms of the absolute magnitudes (when the changes in the AODs are also incorporated) the effect becomes quite dramatic as shown in Fig. 10 for three cases, group 3 (BoB), groups 2 and 5 (predominantly Indian), and group 6 (west Asian and coastal Indian). There is a consistent increase in the net atmospheric forcing (heating) as the transport shifts more to the west (from the BoB regions). Thus, the aerosol radiative forcing over the AS changes significantly with season and even in the given season (intermonsoon); the mean forcing being considerably modified by long-range transport.

6. Summary and conclusions

Continuous measurements of surface, as well as columnar aerosol properties (spectral AOD, size distribution, BC mass concentration, and total aerosol mass concentration) were made over the AS adjoining India (8°–12°N, 72°–77°E) simultaneous with columnar spectral AOD measurements over the peninsular India during the intermonsoon period (March and April 2003) during the ARMEX. The main conclusions of our study are the following.

(i) Mean AODs over the AS (~0.44 at 500 nm) were comparable to those over the coastal land (~0.47), but were lower than the values observed over the semiarid regions of central Indian Peninsula (~0.61).

(ii) The mass concentration of aerosol BC was significantly low over the oceanic regions. It constituted only ~2.2% of the total (composite) aerosol mass concentration, compared to the climatological values of ~6% over the coastal land during the same season, or the reported value over ocean during winter monsoon season. Consequently the atmospheric forcing is reduced to values remarkably lower than those reported for winter season but remain higher than those reported for summer monsoon season.

(iii) Spectral AODs and the Ångström parameters were modified by long-range transport. Mean AODs and β were highest and the spectra were flat with the lowest values of α (~1) when the back trajectories indicated advection from the western landmasses (west Asia, western and coastal India), while the AODs and β were lowest and the spectra were steepest when the trajectories indicated advection from the BoB; the predominantly Indian regions coming in between. The concentration of near-surface aerosols or the mass fraction of BC were however insensitive to the changes in the trajectories.

(iv) The direct, shortwave aerosol forcing efficiencies over the AS during the intermonsoon season, are significantly lower than the values reported for this region during winter season and this is attributed mainly to the reduced mass fraction of BC. Significant intraseasonal variations occur in the forcing, mainly associated with the long-range transport of aerosols. The net atmospheric forcing is found to increase remarkably when there were indications

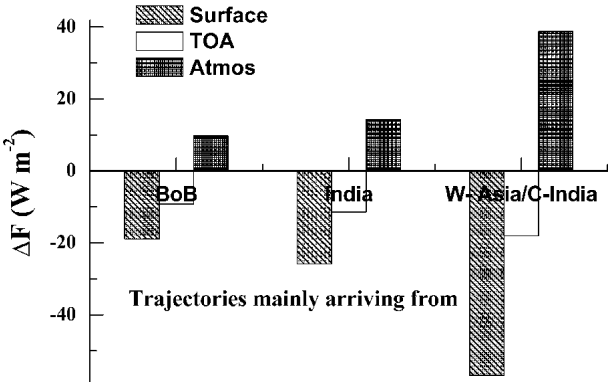

FIG. 10. Variation of the TOA, surface, and atmospheric components of the forcing with respect to the regions from which the advection is predominant as indicated by the back trajectories. Note the significant increase in the atmospheric forcing for the advection from the west Asian regions as compared to those from the BoB and Indian regions.

of transport from the western landmass, in spite of the fact the BC mass fraction remained the same. This is attributed to the impact of mineral dust transported from the arid regions lying to the north and west.

(v) This large heterogeneity in aerosol forcing over the ocean and land at short time scales (with in a season) as well as from season to season have important implications in assessing climate impact.

(vi) AOD showed significant diurnal variations when the advection was mainly across Indian peninsula with a general decrease toward the afternoon. However, the diurnal variations decreased considerably with increased advection of mineral dust (from the west).

Acknowledgments. This study was carried out as a part of Aerosol Climatology and Effects project of ISRO-GBP and Arabian Sea Monsoon Experiment (ARMEX) of the ICRP. The authors are thankful to Department of Science and Technology (DST), Department of Ocean development (DoD), and the chief scientist of the cruise for providing the shipboard facilities. We are thankful to D. R. Sikka and Sulochana Gadgil for providing the opportunity, and R. Sridharan for the constant support. We thank Nazeer Ahmed and R. R. Reddy for providing the spectral AOD values for Anantapur. The authors gratefully acknowledge the NOAA Air resources Laboratory (ARL) for the provision of the HYSPLIT transport and dispersion model and /or READY Web site (available online at http.// www/arl.noaa/gov/ready.html) used in this publication. We thank the reviewers for the useful comments.

REFERENCES

Andreae, M. O., 1995: Climatic effects of changing atmospheric aerosol levels. *World Survey of Climatology,* A. Henderson-Sellers, Ed., Future Climates of the World, Vol. 16, Elsevier, 341–392.

Ångström, A., 1964: The parameters of atmospheric turbidity. *Tellus,* **16,** 64–75.

Asnani, G. C., 1993: *Tropical Meteorology*. Vols. 1 and 2. Indian Institute of Tropical Meteorology, 1202 pp.

Babu, S. S., and K. K. Moorthy, 2002: Aerosol black carbon over a tropical coastal station in India. *Geophys. Res. Lett.,* **29,** 2098, doi:10.1029/2002GL015662.

——, S. K. Satheesh, and K. K. Moorthy, 2002: Aerosol radiative forcing due to enhanced black carbon at an urban site in India. *Geophys. Res. Lett.,* **29,** 1880, doi:10.1029/2002GL015826.

——, K. K. Moorthy, and S. K. Satheesh, 2004: Aerosol black carbon over Arabian Sea during intermonsoon and summer monsoon seasons. *Geophys. Res. Lett.,* **31,** L06104, doi:10.1029/2003GL018716.

Boucher, O., and Coauthors, 1998: Intercomparison of models representing direct shortwave radiative forcing by sulfate aerosols. *J. Geophys. Res.,* **103,** 16 979–16 998.

Capaldo, K., J. J. Corbett, P. Kasibhatala, P. Fischbeck, and S. N. Pandis, 1999: Effects of ship emissions on sulphur cycling and radiative climate forcing over the ocean. *Nature,* **400,** 743–746.

Charlson, R. J., S. E. Schwartz, J. M. Hales, R. D. Cess, J. A. Coakley, J. E. Hansen, and D. J. Hoffman, 1992: Climate forcing by anthropogenic aerosols. *Science,* **255,** 423–430.

Chuang, C. C., J. E. Penner, K. E. Taylor, A. S. Grossman, and J. J. Walton, 1997: An assessment of the radiative effects of anthropogenic sulphate. *J. Geophys. Res.,* **102,** 3761–3778.

Draxler, R. R., and G. D. Rolph, cited 2003: HYSPLIT (Hybrid Single Particle Lagrangian Integrated Trajectory) model access. [Available online at http://www.arl.noaa/gov/ready/hysplit.html.]

Hansen, A. D. A., H. Rosen, and T. Novakov, 1984: Aethalometer—An instrument for the real-time measurement of optical absorption by aerosol particles. *Sci. Total Environ.,* **36,** 191–196.

Hansen, J., M. Sato, and R. Ruedy, 1997: Radiative forcing and climate response. *J. Geophys. Res.,* **102,** 6831–6864.

Haywood, J. M., and K. P. Shine, 1995: The effect of anthropogenic sulphate and soot on the clear sky planetary radiation budget. *Geophys. Res. Lett.,* **22,** 603–606.

——, and V. Ramaswamy, 1998: Global sensitivity studies of the direct radiative forcing due to anthropogenic sulfate and black carbon aerosols. *J. Geophys. Res.,* **103,** 6043–6058.

——, ——, and B. J. Soden, 1999: Tropospheric aerosol climate forcing in clear-sky satellite observations over the oceans. *Science,* **283,** 1299–1303.

Hess, M., P. Koepke, and I. Schultz, 1998: Optical properties of aerosols and clouds: The software package OPAC. *Bull. Amer. Meteor. Soc.,* **79,** 831–844.

Heymsfield, A. J., and G. M. McFarquhar, 2001: Microphysics of INDOEX Clean and Polluted Trade Cumulus Clouds. *J. Geophys. Res.,* **106** (D22), 28 653–28 673.

Houghton, J. T., Y. Ding, D. J. Griggs, M. Noguer, P. J. van der Linden, X. Dai, K. Maskell, and C. A. Johnson, Eds., 2001: *Climate Change 2001: The Scientific Basis.* Cambridge University Press, 881 pp.

Husar, R. B., J. M. Prospero, and L. L. Stowe, 1997: Characterisation of tropospheric aerosols over the oceans with the NOAA advanced very high resolution radiometer optical thickness operational product. *J. Geophys. Res.,* **102,** 16 889–16 909.

Ichoku, C., and Coauthors, 2002: Analysis of the performance characteristics of the five-channel Microtops II Sun photometer for measuring aerosol optical thickness and precipitable water vapor. *J. Geophys. Res.*, **107,** 4179, doi:10.1029/2001JD001302.

Im, J. S., V. K. Saxena, and B. N. Wenny, 2001: An assessment of hygroscopic growth factors for aerosols in the surface boundary layer for computing direct radiative forcing. *J. Geophys. Res.,* **106,** 20 213–20 224.

Jayaraman, A., S. K. Satheesh, A. P. Mitra, and V. Ramanathan, 2001: Latitude gradient in aerosol properties across the Inter-Tropical Convergence Zone: Results from the joint Indo-U.S. study onboard Sagar Kanya. *Curr. Sci.,* **80,** 128–137.

Jha, B., and T. N. Krishnamurti, 1999: Real time meteorological atlas during the INDOEX-199. FSU Rep. 98-09, Florida State University, Tallahassee, FL.

Kamra, A. K., P. Murugavel, S. D. Pawar, and V. Gopalakrishnan, 2001: Background aerosol concentration derived from the atmospheric electric conductivity measurements made over the Indian ocean during INDOEX. *J. Geophys. Res.,* **106,** 28 643–28 651.

Kaufman, Y. J., B. N. Holben, D. Tanre, I. Slutsker, A. Smirnov, and T. F. Eck, 2000: Will aerosol measurements from Terra and Aqua polar orbiting satellites represent the daily aerosol abundance and properties? *Geophys. Res. Lett.,* **27,** 3861–3864.

Kiehl, J. T., and B. P. Briegleb, 1993: The relative roles of sulfate aerosols and greenhouse gases in climate forcing. *Science,* **260,** 311–314.

Krishnamurti, T. N., B. Jha, J. M. Prospero, A. Jayaraman, and V. Ramanathan, 1998: Aerosol and pollutant transport and their

impact on radiative forcing over the tropical Indian Ocean during the January–February 1996 pre-INDOEX cruise. *Tellus,* **50B,** 521–542.

Li, F., and V. Ramanathan, 2002: Winter to summer monsoon variation of aerosol optical depth over the tropical Indian Ocean. *J. Geophys. Res.*, **107,** 4284, doi:10.1029/2001JD000949.

Liou, K. N., 2002: *An Introduction to Atmospheric Radiation*. Academic Press, 583 pp.

Lubin, D., S. K. Satheesh, G. McFarquar, and A. J. Heymsfield, 2002: Longwave radiative forcing of Indian Ocean tropospheric aerosol. *J. Geophys. Res.*, **107,** 8004, doi:10.1029/2001JD001183.

Manghnani, V., S. Raman, D. S. Niyogi, V. Parameswara, J. M. Morrison, S. V. Ramana, and J. V. Raju, 2000: Marine boundary-layer variability over the Indian Ocean during INDOEX (1998). *Bound.-Layer Meteor.*, **97,** 411–430.

Markowicz, K. M., and Coauthors, 2003: Influence of relative humidity on aerosol radiative forcing: An ACE-Asia experiment perspective. *J. Geophys. Res.,* **108,** 8662, doi:10.1029/2002JD003066.

Moorthy, K. K., and A. Saha, 2000: Aerosol study during INDOEX: Observation of enhanced aerosol activity over the Mid Arabian Sea during the northern winter. *J. Atmos. Sol. Terr. Phys.,* **62,** 65–72.

——, and S. K. Satheesh, 2000: Characteristics of aerosols over a remote island, Minicoy in the Arabian Sea: Optical properties and retrieved size characteristics. *Quart. J. Roy. Meteor. Soc.,* **126,** 81–109.

——, ——, and B. V. K. Murthy, 1997: Investigations of marine aerosols over the tropical Indian Ocean. *J. Geophys. Res.,* **102,** 18 827–18 842.

——, A. Saha, B. S. N. Prasad, K. Niranjan, D. Jhurry, and P. S. Pillai, 2001: Aerosol optical depths over peninsular India and adjoining oceans during the INDOEX campaigns: Spatial, temporal, and spectral characteristics. *J. Geophys. Res.,* **106** (D22), 28 539–28 554.

——, S. S. Babu, and S. K. Satheesh, 2003: Aerosol spectral optical depths over the Bay of Bengal: Role of transport. *Geophys. Res. Lett.*, **30,** 1249, doi:10.1029/2002GL016520.

Morys, M., F. M. Mims III, S. Hagerup, S. E. Anderson, A. Baker, J. Kia, and T. Walkup, 2001: Design, calibration and performance of Microtops II handheld ozone monitor and Sun photometer. *J. Geophys. Res.,* **106,** 14 573–14 582.

Neusüß, C., T. Gnauk, A. Plewka, and H. Herrmann, 2002: Carbonaceous aerosol over the Indian Ocean: OC/EC fractions and selected specifications from size-segregated onboard samples. *J. Geophys. Res.,* **107** (D19), 8031, doi:10.1029/2001JD000327.

Pillai, P. S., and K. K. Moorthy, 2001: Aerosol mass-size distributions at a tropical coastal environment: Response to mesoscale and synoptic processes. *Atmos. Environ.,* **35,** 4099–4112.

Pilnis, C., S. N. Pandis, and J. H. Seinfield, 1995: Sensitivity of direct climate forcing by atmospheric aerosols to aerosol size composition. *J. Geophys. Res.,* **100,** 18 739–18 754.

Podgorny, I. A., W. C. Conant, V. Ramanathan, and S. K. Satheesh, 2000: Aerosol modulation of atmospheric and surface solar heating over the tropical Indian Ocean. *Tellus,* **52B,** 947–958.

Posfai, M., J. R. Anderson, P. R. Buseck, and H. Sievering, 1999: Soot and sulfate aerosol particles in the remote marine troposphere. *J. Geophys. Res.,* **104,** 21 685–21 693.

Prospero, J. M., 1979: Mineral and sea salt aerosol concentrations in various ocean regions. *J. Geophys. Res.,* **84,** 725–731.

——, R. J. Charlson, B. Mohnen, R. Jaenicke, A. C. Delany, J. Mayers, W. Zoller, and K. Rahn, 1983: The atmospheric aerosol system—An overview. *Rev. Geophys.,* **21,** 1607–1629.

Ramachandran, S., and A. Jayaraman, 2002: Premonsoon aerosol mass loadings and size distributions over the Arabian Sea and the tropical Indian Ocean. *J. Geophys. Res.*, **107,** 4738, doi:10.1029/2002JD002386.

Ramanathan, V., and Coauthors, 2001: Indian Ocean Experiment: An integrated analysis of the climate forcing and effects of the great Indo-Asian haze. *J. Geophys. Res.,* **106,** 28 371–28 398.

Ricchiazzi, P., S. Yang, C. Gautier, and D. Sowle, 1998: SBDART: A research and teaching software tool for plane-parallel radiative transfer in the earth's atmosphere. *Bull. Amer. Meteor. Soc.,* **79,** 2101–2114.

Russell, P. B., and Coauthors, 2002: Comparison of aerosol single scattering albedos derived by diverse techniques in two North Atlantic experiments. *J. Atmos. Sci.,* **59,** 609–619.

Sakerin, S. M., and D. M. Kabanov, 2002: Spatial inhomogeneities and the spectral behavior of atmospheric aerosol optical depth over the Atlantic Ocean. *J. Atmos. Sci.,* **59,** 484–500.

Satheesh, S. K., and K. K. Moorthy, 1997: Aerosol characteristics over coastal regions of the Arabian Sea. *Tellus,* **49B,** 417–428.

——, and V. Ramanathan, 2000: Large differences in the tropical aerosol forcing at the top of the atmosphere and Earth's surface. *Nature,* **405,** 60–63.

——, and J. Srinivasan, 2002: Enhanced aerosol loading over Arabian Sea during the pre-monsoon season: Natural or anthropogenic? *Geophys. Res. Lett.,* **29,** 1874, doi:10.1029/2002GL015687.

——, V. Ramanathan, X. Li-Jones, J. M. Lobert, I. A. Podgorny, J. M. Prospero, B. N. G. Holben, and N. G. Loeb, 1999: A model for the natural and anthropogenic aerosols over the Tropical Indian Ocean derived from Indian Ocean Experiment Data. *J. Geophys. Res.*, **104** (D22), 27 421–27 440.

——, K. K. Moorthy, and I. Das, 2001: Aerosol optical depths over Bay of Bengal, Indian Ocean and Arabian Sea. *Curr. Sci.,* **81,** 1617–1625.

——, V. Ramanathan, B. N. Holben, K. K. Moorthy, N. G. Loeb, H. Maring, J. M. Prospero, and D. Savoie, 2002: Chemical, microphysical, and radiative effects of Indian Ocean aerosols. *J. Geophys. Res.*, **107,** 4725, doi:10.1029/2002JD002463.

Smirnov, A., and Coauthors, 2002a: Atmospheric aerosol optical properties in the Persian Gulf. *J. Atmos. Sci.,* **59,** 620–634.

——, B. N. Holben, T. F. Eck, I. Slutsker, B. Chatenet, and R. T. Pinker, 2002b: Diurnal variability of aerosol optical depth observed at AERONET (Aerosol Robotic Network) sites. *Geophys. Res. Lett.,* **29,** 2115, doi:10.1029/2002GL016305.

Stamnes, K., S. Tsay, W. Wiscombe, and K. Jayaweera, 1988: Numerically stable algorithm for discrete-ordinate-method radiative transfer in multiple scattering and emitting layered media. *Appl. Opt.,* **27,** 2502–2509.

Taylor, K. E., and J. E. Penner, 1994: Response of the climate system to atmospheric aerosols and green house gases. *Nature,* **369,** 734–737.

Twomey, S., 1977: *Atmospheric Aerosols.* Elsevier, 302 pp.

Vinoj, V., and S. K. Satheesh, 2003: Measurements of aerosol optical depth over Arabian Sea during summer monsoon season. *Geophys. Res. Lett.*, **30,** 1263, doi:10.1029/2002GL016664.

——, S. S. Babu, S. K. Satheesh, K. K. Moorthy, and Y. J. Kaufman, 2004: Radiative forcing by aerosols over the Bay of Bengal region derived from ship borne, island-based, and satellite (Moderate-Resolution Imaging Spectroradiometer) observations. *J. Geophys. Res.*, **109,** D05203, doi:10.1029/2003JD004329.

Wang, J., X. Xia, P. Wang, and S. A. Christopher, 2004: Diurnal variability of dust aerosol optical thickness and Ångström exponent over dust source regions in China. *Geophys. Res. Lett.,* **31,** L08107, doi:10.1029/2004GL019580.

Xu, J., M. H. Bergin, R. Greenwald, and P. B. Russell, 2003: Direct aerosol radiative forcing in the Yangtze delta region of China: Observation and model estimation. *J. Geophys. Res.*, **108,** 4060, doi:10:1029/2002JD002550.